Chinese Chemical Letters 36 (2025) 109769

Contents lists available at ScienceDirect

Chinese Chemical Letters

journal homepage: www.elsevier.com/locate/cclet

A phenylphenthiazide anchored Tb(III)-cyclen complex for fluorescent turn-on sensing of ClO^-

Ya-Ping Liu, Zhi-Rong Gui, Zhen-Wen Zhang, Sai-Kang Wang, Wei Lang, Yanzhu Liu*, Qian-Yong Cao*

School of Chemistry and Chemical Engineering, Nanchang University, Nanchang 330031, China

ARTICLE INFO

Article history:
Received 9 January 2024
Revised 11 March 2024
Accepted 13 March 2024
Available online 14 March 2024

Keywords:
Phenylphenothiazine
Tb(III) complex
AIE
Hypochlorite ion
Sensing

ABSTRACT

A phenylphenothiazine anchored Tb(III)-cyclen complex **PTP-Cy-Tb** for hypochlorite ion (ClO^-) detection has been designed and prepared. **PTP-Cy-Tb** shows a weak Tb-based emission with AIE-characteristics in aqueous solutions. After addition of ClO^-, the fluorescence of **PTP-Cy-Tb** gives a large enhancement for oxidization the thioether to sulfoxide group. The detection limit of **PTP-Cy-Tb** toward ClO^- is as low as 8.85 nmol/L. The sensing mechanism was detailedly investigated by time of flight mass spectrometer (TOF-MS), Fourier transform infrared spectroscopy (FT-IR) and density functional theory (DFT) calculation. In addition, **PTP-Cy-Tb** has been successfully used for on-site and real-time detection of ClO^- in real water samples by using the smartphone-based visualization method and test strips.

Hypochlorite ion (ClO^-) is a key reactive oxygen species (ROS), which is produced by immune cells to fight off foreign bacteria and viruses [1,2]. However, excessive amounts of ClO^- can damage tissues, and cause a range of diseases such as cancer, arthritis, cardiovascular disease, and neurological disease [3–6]. In addition, hypochlorite is the main ingredient in bleach and disinfectants, which is also very important for our daily life. Therefore, selective and sensitive detection of hypochlorite is extremely important.

At present, the methods for detecting ClO^- include colorimetric analysis, electrochemical analysis, chromatographic analysis, nuclear magnetic resonance, and fluorescence probe techniques [7–9]. Among them, fluorescent probes have attracted particular attention for their excellent sensitivity and selectivity, real-time detection, high spectral resolution, and low cost [10,11]. Thus, various fluorescent probes with different recognition sites, such as unsaturated C=C and C=N bonds [12,13], thioether [14,15], amino group [16] and hydrazide [17], have been reported for sensing and detection of ClO^-. However, most of these probes are somewhat hampered by their small Stokes shifts, long response times, and poor water solubility. Therefore, it is essential for development of novel fluorescent probes with simple synthesis and excellent performance for ClO^- ultrafast response.

Luminescent lanthanide complexes, particularly of Eu(III) and Tb(III), have been widely used in sensing field for their inherent advantages such as narrow f-f emission band, long fluorescence lifetime, and large Stokes shift [18,19]. Owing to their long-lifetime emissions, lanthanide complexes are suitable for time-gated luminescence analysis, which can eliminate short-lived background autofluorescence and improve sensitivity and accuracy of probes. Some lanthanide-based probes for sensing of HOCl/OCl^- were also reported [20]. However, most of lanthanide complexes were selected typical aggregation-caused quenching (ACQ) type ligands, which may quench the probes emission in their aggregated state [21]. Recently, the aggregation-induced emission luminogens (AIEgens) demonstrated by Tang *et al.* have been attracted much attention for their particular emission characteristics, *i.e.*, they emit weak luminescence in the solvated molecular state due to the free rotation of the aryl groups, and show strong fluorescence in the aggregated state for restriction the free rotation [22]. Thus, some groups tentatively incorporated the AIEgens into the Ln(III) complexes [23], which can sensitize the Ln(III) center with enhanced luminescence at the aggregated state. The AIE-active Ln(III) complex probes may have potential applications in insoluble water solution for high emission.

In the above context, herein we design and synthesize a novel phenylphenothiazine anchored Tb(III)-cyclen complex **PTP-Cy-Tb** for ClO^- detection (Scheme 1). The phenylphenothiazine antenna was rationally selected for its AIE characteristics [24], and the thioether group in phenothiazine ring is also a good reaction site of ClO^-. While the octadentate macrocyclic polyaminocarboxylate ligand exhibits high binding affinity toward Tb(III), which make the complex high stability in aqueous solution [25,26]. We found that

* Corresponding authors.
E-mail addresses: yzliu@ncu.edu.cn (Y. Liu), cqyong@ncu.edu.cn (Q.-Y. Cao).

https://doi.org/10.1016/j.cclet.2024.109769
1001-8417/

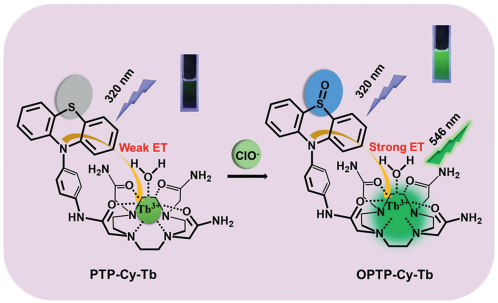

Scheme 1. Proposed detection mechanism of the **PTP-Cy-Tb** probe to ClO^-.

the AIE antenna can sensitize the Tb^{3+} ion fluorescence, and make the **PTP-Cy-Tb** complex a good AIE characteristic. Importantly, **PTP-Cy-Tb** complex shows fluorescence turn-on respond toward ClO^- in aqueous solution for oxidation the thioether group of **PTP-Cy-Tb** to sulfoxide of **OPTP-Cy-Tb**, which makes the energy transfer from ligand to Tb(III) center more effectively. The recognition mechanism and the application of probe were also well discussed.

The detailed synthesis route of ligand **PTP-Cy** and its Tb(III) complex **PTP-Cy-Tb** (Scheme S1 in Supporting information). Briefly, a phenylphenthiazide anchored Tb(III)-cyclen ligand **PTP-Cy** was first prepared from 4-(10*H*-phenothiazin-10-yl)aniline over four steps. $TbCl_3{\cdot}6H_2O$ was coordinated with the AIE fluorophore **PTP-Cy** in CH_3OH solution to obtain the target compound **PTP-Cy-Tb** as a white solid. The structure of ligand **PTP-Cy** was fully characterized by ^1H nuclear magnetic resonance (NMR), ^{13}C NMR and time of flight mass spectrometer (TOF-MS) spectrum (Figs. S1–S7 in Supporting information), while the structure of **PTP-Cy-Tb** can be confirmed by TOF-MS spectrum (Fig. S8 in Supporting information) and Fourier transform-infrared (FT-IR) spectra (Fig. S9 in Supporting information). In the FT-IR spectra, the signal peaks of C=O and C–N in **PTP-Cy** locate at 1679 and 1104 cm^{-1}, respectively. After coordinated with Tb^{3+}, these two peaks show a lower wavenumber shift to 1654 and 1080 cm^{-1}, respectively, indicating that the four N and O atoms are involved in the coordination with Tb^{3+} in **PTP-Cy-Tb** complex.

The absorption spectra of **PTP-Cy** and **PTP-Cy-Tb** in 4-(2-hydroxyethyl)−1-piperazineethanesulfonic acid (HEPES) buffer solution (10 mmol/L, pH 7.4). As shown in Fig. 1a, **PTP-Cy** shows an absorption peak at 306 nm, while this ligand-based absorption red shifts to 312 nm in **PTP-Cy-Tb**. This may be attributed to the increased degree of electron delocalizetion after coordination of the ligand **PTP-Cy** with Tb^{3+}, leading to a greater range of π-electron activity in the complex. Therefore, the energy level transition energy of **PTP-Cy-Tb** molecular orbital decreases, resulting in a red-shift of the absorption peak. Then, we tested emission spectra of **PTP-Cy** and **PTP-Cy-Tb** in HEPES buffer solution (10 mmol/L, pH 7.4) (Fig. 1b). With excitation at 320 nm, **PTP-Cy** exhibits two fluorescence emission peaks at 374 and 448 nm, respectively. The emission at 374 nm can be attributed to the localized excited (LE) state in the molecules, while the long-wavelength emission at 448 nm may originate from the intramolecular charge transfer (ICT) from phenothiazine to benzene moiety [27]. In the emission spectra of **PTP-Cy-Tb**, the ligand-based emission can also be observed, but its intensity largely decreases. In addition, the Tb^{3+} based emission peaks at 491 nm ($^5D_4 \rightarrow {}^7F_6$), 546 nm ($^5D_4 \rightarrow {}^7F_5$), 586 nm ($^5D_4 \rightarrow {}^7F_4$) and 621 nm ($^5D_4 \rightarrow {}^7F_3$) were observed. In order to distinguish between ligand fluorophore and Tb(III) luminescence, we tested the time-gated emission spectra of **PTP-Cy-Tb** with a delay time of 0.1 ms, which exhibited clear Tb(III) emission (Fig. S10 in Supporting information). The above results confirm that Tb^{3+} emission was sensitized through **PTP-Cy**.

The fluorescence lifetime of **PTP-Cy-Tb** was measured in H_2O and D_2O. As shown in Table S1 and Fig. S11 (Supporting information), the fluorescence lifetime of **PTP-Cy-Tb** in water was 0.51 ms, while value in D_2O was 0.59 ms. According to the formula $q = 5.0 \times (K_{H_2O} - K_{D_2O} - 0.06)$ [28], we derived the number of ligand water molecules of **PTP-Cy-Tb** to be one.

Owing to the butterfly shape of the core ring, phenothiazine derivatives often show AIE features [29,30], which also observed in **PTP-Cy** ligand (Fig. S12 in Supporting information). Thus, we investigated the AIE properties of **PTP-Cy-Tb** complex in toluene/DMSO mixture, because it shows good solubility in DMSO, but is insoluble in toluene. As shown in Fig. 1c and Fig. S13 (Supporting information), **PTP-Cy-Tb** shows weak emission in DMSO. Upon increasing the fraction of toluene, its emission gradually increased and attained the maximum intensity in 100% toluene solution, due to the formation of molecular aggregates. Thus, **PTP-Cy-Tb** complex exhibits typical AIE characteristic.

The sensing ability of **PTP-Cy-Tb** toward ClO^- was then investigated by emission spectra in HEPES buffer solution (10 mmol/L, pH 7.4). Firstly, the respond time of probe was investigated by the time-dependent fluorescence experiment of **PTP-Cy-Tb** (20 μmol/L)

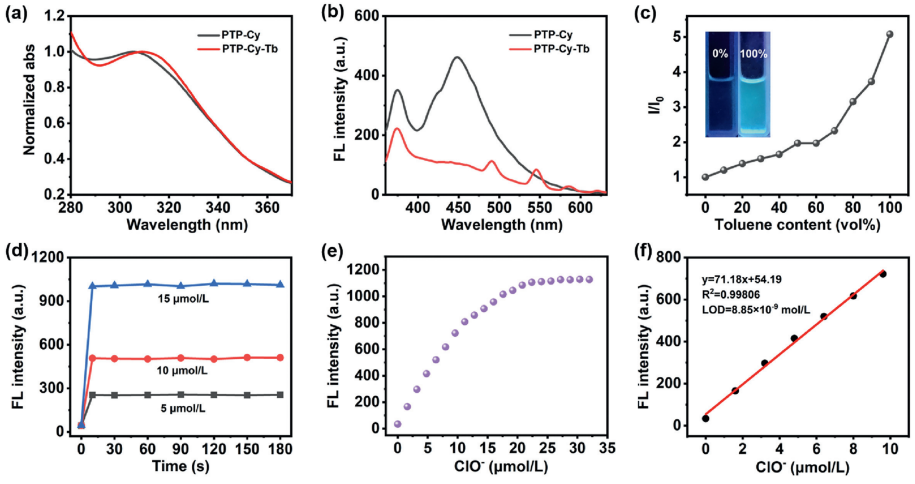

Fig. 1. Normalized absorption (a) and emission (b) spectra of **PTP-Cy** and **PTP-Cy-Tb** ($c = 20$ μmol/L, $\lambda_{ex} = 320$ nm). (c) The relative emission intensity (I/I_0) of **PTP-Cy-Tb** at 546 nm *versus* the fraction of the Toluene/DMSO mixtures ($\lambda_{ex} = 320$ nm). Inset: Fluorescence in DMSO and in toluene. (d) Fluorescence (FL) intensity of **PTP-Cy-Tb** at 546 nm (20 μmol/L) with adding different concentrations of ClO^- *versus* the reaction time ($\lambda_{ex} = 320$ nm). (e) Fluorescence intensity of **PTP-Cy-Tb** at 546 nm (20 μmol/L) with increasing concentration of ClO^- (0–32 μmol/L). (f) Linear relationship between fluorescence intensity and ClO^- concentration.

with different concentrations of ClO^- (5, 10 and 20 μmol/L). As shown in Fig. 1d, the fluorescence intensity of **PTP-Cy-Tb** for all three concentrations of ClO^- increased quickly and saturated within 10 s, and then remained almost constant with time. Therefore, 10 s was chosen as the optimal reaction time for **PTP-Cy-Tb** and ClO^-. Subsequently, the fluorescence intensity of **PTP-Cy-Tb** *versus* the concentration of ClO^- was recorded by normal emission titration and also time-gated emission spectra. As shown in Fig. 1e and Figs. S14 and S15 (Supporting information), upon increasing the concentration of ClO^- from 0 to 32 μmol/L, both the ligand-base emission at 375 nm and Tb^{3+}-central emission at 491, 546, 586 and 621 nm gradually increased and saturated after the addition of 22.4 μmol/L ClO^-, with the maximum peak at 546 nm a 33-fold enhancement. The fluorescence response can be easily observed by the naked eyes, with the fluorescent color change from dark emission to strong green emission under a handle ultraviolet (UV) light irradiation. In addition, there was a good linear relationship between the fluorescence intensity at 546 nm and the ClO^- concentration in the range of 0–9.6 μmol/L (Fig. 1f), and the limit of detection (LOD) was determined to be 8.85 nmol/L according to the $3\sigma/K$ rule [31].

The absorption of **PTP-Cy-Tb** before and after addition of ClO^- was also carried out (Fig. S16 in Supporting information). After addition of ClO^-, two new absorption peaks at 302 and 337 nm appeared. In addition, the fluorescence lifetime of **PTP-Cy-Tb** after addition of ClO^- were also investigated (Table S1 and Fig. S17 in Supporting information). The calculated number of coordination water was also one, indicating that the Tb^{3+} coordination central is basically unchanged before and after the addition of ClO^-. Thus, **PTP-Cy-Tb** can be used for absorption and emission detection of ClO^-.

The fluorescent sensing selectivity of **PTP-Cy-Tb** (20 μmol/L) was then evaluated by addition same amount (100 μmol/L) of various analytes. As shown in Fig. 2a and Fig. S18 (Supporting information), there is a clear fluorescence enhancement at 546 nm in the presence of ClO^-, while the addition of other analytes leads to barely fluorescence change. In addition, competition experiments were also performed by first adding 100 μmol/L of other analytes, followed by the addition of same amount of ClO^- to **PTP-Cy-Tb** solution (20 μmol/L). As shown in Fig. 2b, **PTP-Cy-Tb** still showed a good fluorescence enhancement of ClO^- under the same test conditions. These experimental results indicate that **PTP-Cy-Tb** has good selectivity and anti-interference effect on ClO^-.

The appropriate pH range is crucial for the application of fluorescent probes. Thus, we also investigated the effects of pH on recognition behaviors of **PTP-Cy-Tb** toward ClO^-. As shown in Fig. 2c, **PTP-Cy-Tb** still exhibits a good sensing ability toward ClO^- in wide pH range from 5.0 to 9.0, which can be used in environmental and physiological condition.

The highly sensitive and selective sensing of **PTP-Cy-Tb** toward ClO^- may be attributed the strong oxidation property of ClO^-, which can oxidize **PTP-Cy-Tb** to **OPTP-Cy-Tb**. This transformation can be verified by mass spectra and FT-IR. As shown in Fig. S19 (Supporting information), we found only the TOF-MS (*m/z*) signal of **OPTP-Cy-Tb** at 848.3553 after reaction of **PTP-Cy-Tb** with ClO^-. In addition, a strong FT-IR peak at 979 cm^{-1} appears after addition of ClO^- (Fig. S20 in Supporting information), which further confirmed the formation of the S=O bond.

Subsequently, we calculated the energy transfer efficiency of the pre-oxidized ligand **PTP-Cy** and the post-oxidized ligand **OPTP-Cy** to the Tb^{3+} ion central. As we all known, the antenna effect of **PTP-Cy-Tb**/**OPTP-Cy-Tb** complex involves two steps: first the singlet excited state of ligand **PTP-Cy/OPTP-Cy** undergoes intersystem crossing to the longer-lived triplet excited state ($S_1 \rightarrow T_1$, ΔE_1) after absorption photons; in the second step, the relatively long lifetime T_1 is then transferred to the Tb^{3+} excited states ($T_1 \rightarrow Tb\ ^5D_4$ excited state, 20,500 cm^{-1}) [32]. Both the energy gap of ΔE_1 and ΔE_2 will affect the antenna effect procedure, in which the ΔE_1 should be greater than 5000 cm^{-1} based on the Reinhold's empirical rule, while ΔE_2 must be above 3500 cm^{-1} to inhibit reversible energy transfer [33,34]. We used the density functional theory (DFT) calculation to get the S_1 and T_1 energy level of **PTP-Cy** and **OPTP-Cy**. As shown in Fig. 2d, presents the molecular orbital diagrams of lowest unoccupied molecular orbital (LUMO) and highest occupied molecular orbital (HOMO) of **PTP-Cy** and **OPTP-Cy**, and their energy levels (Fig. 2e and Table S2 in Supporting information). The ΔE_1 values of **PTP-Cy** and **OPTP-Cy** were found to be 3996 and 5145 cm^{-1}, respectively, indicating that the intersys-

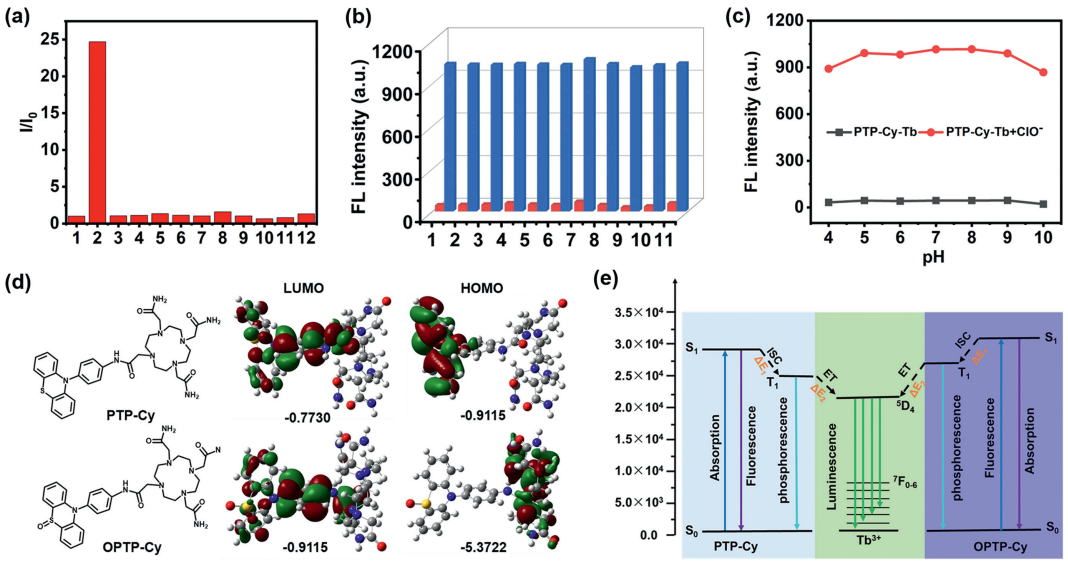

Fig. 2. (a) FL histograms after addition of different analytes (100 μmol/L): 1-blank, 2-ClO^-, 3-F^-, 4-CN^-, 5-NO_2^-, 6-NO_3^-, 7-CH_3COO^-, 8-CO_3^{2-}, 9-H_2O_2, 10-S^{2-}, 11-SO_3^{2-}, 12-SO_4^{2-}. λ_{ex} = 320 nm. (b) The FL intensity of **PTP-Cy-Tb** (c = 20 μmol/L) at 546 nm with addition of 100 μmol/L different analytes (red bar) and then addition of 100 μmol/L ClO^- (blue bar): 1-blank, 2-F^-, 3-CN^-, 4-NO_2^-, 5-NO_3^-, 6-CH_3COO^-, 7-CO_3^{2-}, 8-H_2O_2, 9-S^{2-}, 10-SO_3^{2-}, 11-SO_4^{2-}. (c) FL intensity before and after addition of ClO^- (100 μmol/L) at different pH values. λ_{ex} = 320 nm. (d) The LUMO and HOMO orbital diagrams of **PTP-Cy** and **OPTP-Cy**. (e) Schematic representation of the energy transfer process of **PTP-Cy-Tb** and **OPTP-Cy-Tb**. ISC, intersystem crossing; ET, energy transfer; S, singlet; T, triplet.

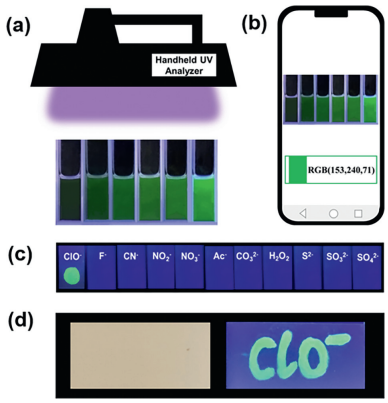

Fig. 3. (a) Fluorescence images with addition of ClO^- (0–10 μmol/L). (b) RGB values analysis of fluorescence images. (c) Fluorescent photographs of different analytes added dropwise to the silica gel plates. (d) Color changes of silica gel plates under visible light (left) and 365 nm UV light (right).

tem crossing from S_1 to T_1 of **OPTP-Cy** is more effective for antenna effect procedure than that of **PTP-Cy**. Meanwhile, the ΔE_2 values of **PTP-Cy-Tb** and **OPTP-Cy-Tb** were 3724 and 5732 cm^{-1}, respectively. Thus, the T_1 state of both ligands can effectively sensitize the excited state of Tb^{3+}. Combining these two constraints, we can rationalize that the **OPTP-Cy** ligand gives more efficient antenna effect to Tb^{3+} center than **PTP-Cy**, which make **PTP-Cy-Tb** a fluorescence turn-on response after reaction with ClO^-.

We also compared **PTP-Cy-Tb** with some previous reported probes of ClO^- (Table S3 in Supporting information). It clearly demonstrates that **PTP-Cy-Tb** shows some advantages with high selectivity, rapid response, large Stokes shift, and better biocompatibility.

The practical application of **PTP-Cy-Tb** for detection of environmental ClO^- was evaluated. We chose three real water samples (Tap water, Qianhu Lake and Ganjiang River) for the detection of ClO^- content. Different concentrations of ClO^- (0, 2, 4 and 8 μmol/L) were added to water samples containing 20 μmol/L **PTP-Cy-Tb**. As shown in Table S4 (Supporting information), ClO^- was not detected in the free real water, but can be observed with almost the same values as the addition ClO^- concentrations. The recoveries were in the range of 96.88%–104.50%, with the relative standard deviations (RSD) lower than 4.98%. These experimental data show that the **PTP-Cy-Tb** probe can be used for the detection of actual water samples in the environment.

Meanwhile, we built a smartphone-assisted rapid detection system of ClO^- for its portable detection, simple and low cost. As shown in Figs. 3a and b, under UV light (365 nm), the solution gradually changes from colorless to green with increasing the concentration of ClO^- (0–10 μmol/L). We obtain the corresponding color information (RGB values) in the fluorescent image through the WeChat color recognition device on the smartphone. The G/G_0 (G_0 and G are the brightness of G channel before and after the addition of ClO^-) can be used as a parameter for ClO^- quantification. As shown in Fig. S21 (Supporting information), there is a linear relationship between G/G_0 and ClO^- concentration (0–10 μmol/L), and the calculated LOD is 51.7 nmol/L. This indicates that the **PTP-Cy-Tb** can be used for real-time and visualized detection of ClO^-.

To investigate the on-site detection of ClO^-, we further developed silica gel plates impregnated with **PTP-Cy-Tb** as test strips. As shown in Fig. 3c, a drop of ClO^- solution (20 μmol/L) was placed on the pretreated silica gel plate, which emitted green fluorescence under UV light (365 nm). In contrast, dropwise addition of other analytes (20 μmol/L) did not fluoresce. Subsequently, we wrote with ClO^- on a pretreated silica gel plate, which showed green fluorescent fonts under UV light (365 nm) (Fig. 3d), whereas under visible light there was no color change. Therefore, **PTP-Cy-Tb** pretreated silica gel plates have the potential to safely and efficiently detect ClO^-.

In summary, we design and synthesize a new phenylphenthiazide anchored Tb(III)-cyclen complex **PTP-Cy-Tb** for ClO^- detection. We found that the AIE-based phenylphenthiazide fluorephore can sensitize Tb(III) center, which makes the **PTP-Cy-Tb** complex also a good AIE characteristics. **PTP-Cy-Tb** shows a good fluorescence turn-on response toward ClO^- over other test species, and the detection limit was found to be 8.85 nmol/L. The TOF-MS and FT-IR experiment confirm that the addition of ClO^- can oxidize the thioether group of **PTP-Cy-Tb** to get the sulfoxide **OPTP-Cy-Tb** complex. The DFT calculations analysis reveal that **OPTP-Cy** ligand gives more efficient antenna effect to Tb(III) center than **PTP-Cy**, which make **PTP-Cy-Tb** a fluorescence turn-on response after reaction with ClO^-. **PTP-Cy-Tb** can detect of ClO^- in real water samples, and the on-site and real-time detection methods were also obtained *via* the smartphone-assisted visualization method and test strips derived from **PTP-Cy-Tb**. This design strategy may be applied to other rare earth fluorescence probes for detecting ClO^- and other molecules with high selectivity and sensitivity.

Declaration of competing interest

The authors declare that they have no known competing financial interests or personal relationships that could have appeared to influence the work reported in this paper.

Acknowledgments

This work was supported by the National Nature Science Foundation of China (Nos. 22061028 and 22361028) and Jiangxi Provincial Natural Science Foundation (No. 20224ACB203012).

Supplementary materials

Supplementary material associated with this article can be found, in the online version, at doi:10.1016/j.cclet.2024.109769.

References

[1] X.Q. Chen, F. Wang, J.Y. Hyun, et al., Chem. Soc. Rev. 45 (2016) 2976–3016.
[2] Y. Koide, Y. Urano, K. Hanaoka, T. Terai, T. Nagano, J. Am. Chem. Soc. 133 (2011) 5680–5682.
[3] C.Y. Chu, X.M. Lyu, Z.X. Wang, et al., Chem. Eng. J. 402 (2020) 126125.
[4] L.J. Gui, J. Yan, J.Y. Zhao, et al., Biosens. Bioelectron. 240 (2023) 115660.
[5] Q.L. Liu, M. Xiao, H.C. Ding, et al., Dyes. Pigm. 215 (2023) 111194.
[6] W. Ahmad, B. Ijaz, K. Shabbiri, et al., J. Biomed. Sci. 24 (2017) 76.
[7] K.J. Wang, D.Z. Xi, C.T. Liu, et al., Chin. Chem. Lett. 31 (2020) 2955–2959.
[8] X.J. Hea, H. Chen, C.C. Xu, et al., J. Hazard. Mater. 388 (2020) 122029.
[9] Y. Zhao, X.Q. Yu, X. Liu, et al., Anal. Chem. 95 (2023) 7170–7177.
[10] J.T. Hou, N. Kwon, S. Wang, et al., Coord. Chem. Rev. 450 (2022) 214232.
[11] Z.Y. Hu, X.Y. Chen, Y.S. Yang, et al., Coord. Chem. Rev. 501 (2024) 215562.
[12] J.S. Lan, L. Liu, R.F. Zeng, et al., Chem. Commun. 56 (2020) 1219–1222.
[13] Y. Zhou, H. Xu, Q.X. Li, et al., Org. Biomol. Chem. 21 (2023) 1270–1274.
[14] A.S. Zheng, H. Liu, C.H. Peng, et al., Talanta 226 (2021) 122152.
[15] H.J. Wang, W.W. Xing, Z.H. Yu, Chin. Chem. Lett. 35 (2024) 109183.
[16] B.C. Zhu, L. Wu, M. Zhang, et al., Biosens. Bioelectron. 107 (2018) 218–223.
[17] G.J. Mao, Y.Y. Wang, W.P. Dong, et al., Spectrochim. Acta A: Mol. Biomol. Spectrosc. 249 (2021) 119326.
[18] M.C. Heffern, L.M. Matosziuk, T.J. Meade, Chem. Rev. 114 (2014) 4496–4539.
[19] I.F. Costa, L. Blois, T.B. Paolini, et al., Coord. Chem. Rev. 502 (2024) 215590.
[20] L. Tian, H. Ma, B. Song, et al., Talanta 212 (2020) 120760.
[21] J.C. Han, Z.Y. Zhang, D.D. Liu, X. Wang, Chem. Commun. 59 (2023) 90–93.
[22] J. Li, J.X. Wang, H.X. Li, et al., Chem. Soc. Rev. 49 (2020) 1144–1172.
[23] Z.C. Zhu, B. Song, J.L. Yuan, C.L. Yang, Adv. Sci. 3 (2016) 1600146.
[24] J.Y. Zhang, M.N. Zhu, Y.X. Lu, et al., Chem. Eur. J. 28 (2022) e202200458.
[25] S. Aoki, H. Kawatani, T. Goto, E. Kimura, M. Shiro, J. Am. Chem. Soc. 123 (2001) 1123–1132.
[26] H.R. Lei, J. Liu, J.L. Yan, S.H. Lu, Y. Fang, ACS Appl. Mater. Interfaces 6 (2014) 13642–13647.

[27] H. Tanaka, K. Shizu, H. Nakanotani, C. Adachi, J. Phys. Chem. C 118 (2014) 15985–15994.
[28] J. Liu, M. Morikawa, N. Kimizuka, J. Am. Chem. Soc. 133 (2011) 17370–17374.
[29] J. Yang, J.W. Qin, P.Y. Geng, et al., Angew. Chem. 130 (2018) 14370–14374.
[30] X.G. Song, S.G. Shen, M.Y. Lu, Y. Wang, Y. Zhang, Chin. Chem. Lett. 35 (2024) 109118.
[31] J.M. Qin, X. Li, Q.Y. Cao, et al., Chin. Chem. Lett. 35 (2024) 108925.
[32] L. Yu, L.X. Feng, L. Xiong, et al., J. Hazard. Mater. 434 (2022) 128914.
[33] X.Z. Xie, Y.R. Zhang, Y.J. Wu, X.B. Yin, Y. Xia, J. Phys. Chem. C 127 (2023) 1220–1228.
[34] H.Q. Yin, X.Y. Wang, X.B. Yin, J. Am. Chem. Soc. 141 (2019) 15166–15173.